

## RESEARCH ARTICLE SUMMARY

## MICROBIOLOGY

# The lysosomal Rag-Ragulator complex licenses RIPK1- and caspase-8-mediated pyroptosis by *Yersinia*

Zengzhang Zheng<sup>†</sup>, Wanyan Deng<sup>†</sup>, Yang Bai<sup>†</sup>, Rui Miao<sup>†</sup>, Shenglin Mei, Zhibin Zhang, Youdong Pan, Yi Wang, Rui Min, Fan Deng, Zeyu Wu, Wu Li, Pengcheng Chen, Tianchi Ma, Xiwen Lou, Judy Lieberman\*, Xing Liu\*

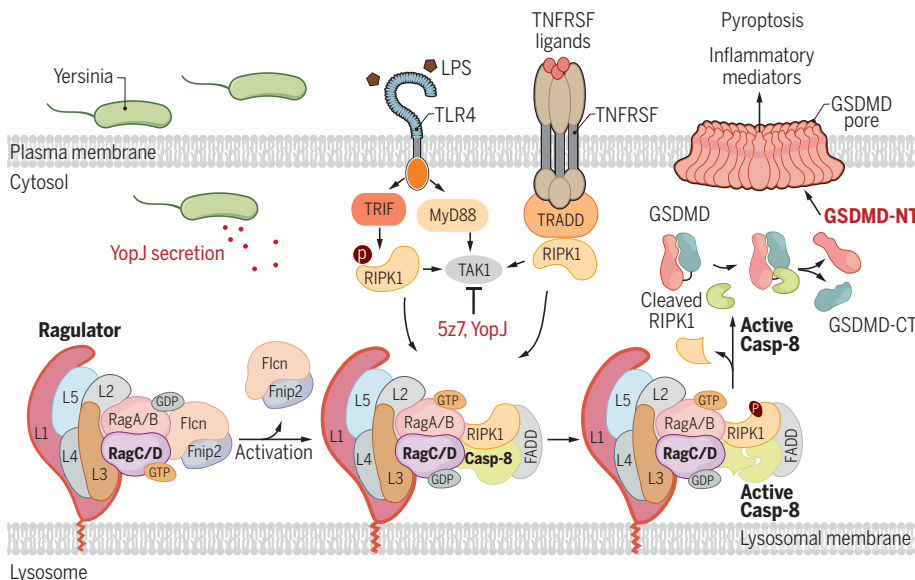
**INTRODUCTION:** An inflammatory innate immune response is a first line of host defense against invading pathogens. Inflammation recruits immune cells to the infection site and activates protective adaptive immune responses. Invasive bacteria have evolved multiple ways to interfere with host innate immune signaling to facilitate infection. The *Yersinia* effector protein YopJ suppresses proinflammatory cytokine production by inhibiting transforming growth factor- $\beta$ -activated kinase 1 (TAK1) and nuclear factor  $\kappa$ B (NF- $\kappa$ B) activation. To counteract this virulence factor, host cells initiate receptor-interacting serine-threonine protein kinase 1 (RIPK1)-dependent caspase-8-directed gasdermin D (GSDMD) cleavage and inflammatory cell death (pyroptosis) when TAK1 is inhibited. However, how the RIPK1-caspase-8-GSDMD axis is instructed during *Yersinia* infection is unclear.

**RATIONALE:** The best-studied mechanism by which pathogens stimulate inflammatory cell death involves triggering cytosolic sensors, called inflammasomes, which activate inflammatory caspases (1/4/5/11) to process proinflammatory cytokines and cause pyroptosis. Inflammatory caspase cleavage of GSDMD causes cell membrane pores that mediate both pyroptosis and proinflammatory cytokine secretion. An alternate pyroptotic pathway, mediated by activation of RIPK1 and caspase-8, is triggered when the YopJ virulence factor secreted during pathogenic *Yersinia* infection blocks TAK1 activation. To determine the molecular mechanisms underlying *Yersinia* activation of RIPK1-caspase-8-dependent pyroptosis, we performed a genome-wide CRISPR screen using Cas9-expressing immortalized mouse bone marrow-derived macrophages infected with a genome-wide library of single-guide RNA-encoding lentiviruses. The genomes of cells

resistant to caspase-8- or caspase-11-dependent pyroptosis were sequenced to identify the knocked-out genes required for pyroptosis.

**RESULTS:** The screen identified multiple genes in the lysosomal membrane-anchored Folliculin (Flcn)-Folliculin-interacting protein 2 (Fnip2)-Rag-Ragulator complex as necessary for caspase-8- but not caspase-11-mediated pyroptosis. Deficiency of Rag-Ragulator complex genes rendered cells highly resistant to TAK1 inhibition-triggered pyroptosis, indicating a critical and unexpected role of the lysosomal membrane-tethered Rag-Ragulator supercomplex in RIPK1-dependent caspase-8-directed pyroptosis. In response to pathogenic *Yersinia* or its mimic [lipopolysaccharide (LPS) plus TAK1 inhibitor], a Fas-associated death domain (FADD)-RIPK1-caspase-8-containing complex was recruited to lysosomal membrane-tethered Rag-Ragulator. Activation of RIPK1 phosphorylation, caspase-8 activation, and pyroptosis depended on Rag guanosine triphosphatase (GTPase) activity and Rag-Ragulator lysosomal binding but was independent of the mechanistic target of rapamycin complex 1 (mTORC1), a well-known Rag-Ragulator-regulated complex. By contrast, Rag-Ragulator did not regulate canonical or non-canonical inflammasome-triggered pyroptosis.

**CONCLUSION:** Our study revealed an instructive role of metabolic signaling in directing TAK1 inhibition-induced pyroptosis during a pathogenic bacterial infection. Rag-Ragulator is a well-known critical regulator of cellular responses to changes in nutrient availability and metabolism. Here, Rag-Ragulator served as a platform for activating a FADD-RIPK1-caspase-8 complex formed in response to Toll-like receptor (TLR) or tumor necrosis factor receptor (TNFR) ligation. Rag GTPase activity was critical for triggering the pathway. The role found here for Rag-Ragulator in pyroptosis expands its known roles in metabolic regulation to include regulation of the response to pathogenic infection. Rag-Ragulator monitors both metabolism and infection to serve as a central hub for helping to decide whether available nutrients are adequate for cell proliferation and if an infected cell should die and send out inflammatory danger signals. Future studies can further explore the conditions that stimulate caspase-8-mediated pyroptosis and provide more mechanistic details of how it is regulated, as well as investigate whether manipulating this pathway could have therapeutic benefit. ■



**Rag-Ragulator serves as a platform for activating a FADD-RIPK1-caspase-8 complex to trigger pyroptosis in response to TLR and TNFR ligation.** When TAK1 is inhibited by the *Yersinia* effector YopJ or its mimic 5z-7-oxozeaenol (5z7), a FADD-RIPK1-caspase-8-containing complex is recruited to lysosome-tethered Rag-Ragulator, which activates caspase-8- and GSDMD-dependent pyroptosis. TNFRSF, TNFR superfamily; L1-5, Lamtor1-5.

The list of author affiliations is available in the full article online.  
\*Corresponding author. Email: judy.lieberman@childrens.harvard.edu (J.L.); xingliu@ips.ac.cn (X.L.)  
<sup>†</sup>These authors contributed equally to this work.  
Cite this article as Z. Zheng *et al.*, *Science* 372, eabg0269 (2021). DOI: 10.1126/science.abg0269

**S** READ THE FULL ARTICLE AT  
<https://doi.org/10.1126/science.abg0269>

## RESEARCH ARTICLE

## MICROBIOLOGY

# The lysosomal Rag-Ragulator complex licenses RIPK1- and caspase-8-mediated pyroptosis by *Yersinia*

Zengzhang Zheng<sup>1,2†</sup>, Wanyan Deng<sup>1,2†</sup>, Yang Bai<sup>2,3†</sup>, Rui Miao<sup>4,5†</sup>, Shenglin Mei<sup>6</sup>, Zhibin Zhang<sup>4,5</sup>, Youdong Pan<sup>7</sup>, Yi Wang<sup>8</sup>, Rui Min<sup>2,3</sup>, Fan Deng<sup>2,3</sup>, Zeyu Wu<sup>2,3</sup>, Wu Li<sup>1,2</sup>, Pengcheng Chen<sup>2</sup>, Tianchi Ma<sup>2</sup>, Xiwen Lou<sup>2</sup>, Judy Lieberman<sup>4,5\*</sup>, Xing Liu<sup>1,2\*</sup>

Host cells initiate cell death programs to limit pathogen infection. Inhibition of transforming growth factor- $\beta$ -activated kinase 1 (TAK1) by pathogenic *Yersinia* in macrophages triggers receptor-interacting serine-threonine protein kinase 1 (RIPK1)-dependent caspase-8 cleavage of gasdermin D (GSDMD) and inflammatory cell death (pyroptosis). A genome-wide CRISPR screen to uncover mediators of caspase-8-dependent pyroptosis identified an unexpected role of the lysosomal folliculin (FLCN)-folliculin-interacting protein 2 (FNIP2)-Rag-Ragulator supercomplex, which regulates metabolic signaling and the mechanistic target of rapamycin complex 1 (mTORC1). In response to *Yersinia* infection, Fas-associated death domain (FADD), RIPK1, and caspase-8 were recruited to Rag-Ragulator, causing RIPK1 phosphorylation and caspase-8 activation. Pyroptosis activation depended on Rag guanosine triphosphatase activity and lysosomal tethering of Rag-Ragulator but not mTORC1. Thus, the lysosomal metabolic regulator Rag-Ragulator instructs the inflammatory response to *Yersinia*.

**W**hen mucosal and immune sentinel cells sense invasive infection or other danger signals, they activate the assembly of large multiprotein complexes called inflammasomes that recruit inflammatory caspases (caspase-1, caspase-4, caspase-5, and caspase-11), which become auto-activated by proximity (1–3). The activated pro-inflammatory caspases then cleave gasdermin D (GSDMD) in the cytosol to liberate an N-terminal fragment that assembles into cell membrane pores to cause an inflammatory cell death called pyroptosis, in which the cell membrane is rapidly permeabilized to release inflammatory mediators (4–9). Caspase-1 also processes the pro-inflammatory interleukin-1 (IL-1) family cytokines, which lack a conventional secretion signal, and the processed inflammatory cytokines are then

released through GSDMD pores (10, 11). Pyroptosis and IL-1 family cytokines recruit and activate immune cells to the site of infection to orchestrate host defense against invading pathogens. During pathogenic *Yersinia* infection, the *Yersinia* effector protein YopJ inhibits transforming growth factor- $\beta$ -activated kinase 1 (TAK1) or I $\kappa$ B kinase (IKK) to trigger an alternate pyroptotic pathway mediated by Toll-like receptors (TLRs) or death receptors that instigate the formation of a complex involving the adapter Fas-associated death domain (FADD) and receptor-interacting serine-threonine protein kinase 1 (RIPK1) and recruitment and activation of caspase-8, which cleaves GSDMD (12, 13). Blockade of TAK1 kinase activity with the specific inhibitor 5z-7-oxozeaenol (5z7) mimics the effect of YopJ and pathogenic *Yersinia* infection to cause RIPK1-caspase-8-dependent GSDMD-mediated pyroptosis in the presence of TLR ligands or tumor necrosis factor- $\alpha$  (TNF- $\alpha$ ). However, not much is known about how this alternative caspase-8-dependent pyroptotic pathway is activated or regulated.

To determine the molecular mechanisms underlying activation of RIPK1-caspase-8-dependent pyroptosis during *Yersinia* infection, we performed an unbiased genome-wide CRISPR screen. We infected Cas9-expressing immortalized mouse bone marrow-derived macrophages (iBMDMs) with lentiviruses encoding a library of single-guide RNAs (sgRNAs) and treated them with extracellular lipopolysaccharide (LPS)/5z7 to trigger caspase-8-dependent pyroptosis or electroporated them with LPS to trigger caspase-11-mediated GSDMD

cleavage for comparison (Fig. 1A). Surviving cells were isolated and retreated twice more to enrich for pyroptosis-resistant cells. The genomes of resistant cells were sequenced to identify enriched sgRNAs that knocked out genes required for pyroptosis. The screen identified multiple genes in the lysosomal membrane-anchored folliculin (Fln)-folliculin-interacting protein 2 (Fnip2)-Rag-Ragulator complex as necessary for caspase-8-mediated pyroptosis but not caspase-11-mediated pyroptosis.

## Genome-wide CRISPR screen identifies the Rag-Ragulator complex as critical for pyroptosis induced by LPS/5z7 treatment

We identified several sgRNAs enriched in cells that survived three sequential exposures to stimuli that triggered caspase-8- or caspase-11-dependent pyroptosis compared with medium-treated control cells (Fig. 1, A to C, and fig. S1). Only a few sgRNA target genes were enriched in cells that survived both caspase-8- and caspase-11-mediated pyroptosis. Cells that survived LPS transfection were significantly enriched for sgRNAs designed to knock out *Gsdmd*, *Casp-11*, and *Irf2*, all known genes implicated in the non-canonical inflammasome pathway, including the gene encoding Irf2, which transcriptionally activates *Gsdmd* expression (14). Caspase-8-induced pyroptosis-resistant cells were highly enriched for sgRNAs targeting genes involved in tumor necrosis factor receptor (TNFR) signaling, mitochondrial electron transport chain (ETC) complex I, and the lysosome-associated Rag-Ragulator complex. The 27 most enriched sgRNAs, which were increased 164- to 2500-fold compared with mock-treated cells, included four sgRNAs targeting the gene encoding TNFR1; eight sgRNAs targeting four genes encoding subunits of ETC complex I (Ndufa6, Ndufa13, Ndufa4, and Ndufa9), and 15 sgRNAs targeting genes encoding five components of the Rag-Ragulator supercomplex (Lamtor1, Lamtor4, RagC, Fln, and Fnip2), which serves as a platform for recruiting Raptor-mTOR (the mechanistic target of rapamycin) to the lysosomal surface and regulating its activation (15). The recovery of TNFR1 sgRNAs in LPS/5z7-treated, but not LPS-transfected, surviving cells confirmed the selectivity of the screen. The identification of ETC complex I gene sgRNAs was not surprising because mitochondrial reactive oxygen species, of which ETC complex I is a major source, have been implicated in augmenting GSDMD pore formation (16, 17). By comparison, neither *Casp-8*- nor *Gsdmd*-targeting guides were enriched, likely because deficiency of caspase-8 or *Gsdmd* could lead to Ripk3-dependent or *Gsdme*-directed cell death (18–20). The Rag-Ragulator supercomplex is composed of nine subunits: Ragulator, a pentameric scaffold (Lamtor1–5) that tethers the complex to the lysosomal membrane by lipidation of Lamtor1 (21, 22); two Rag GTPases (GTP-loaded RagA or

<sup>1</sup>The Joint Center for Infection and Immunity between Guangzhou Institute of Pediatrics, Guangzhou Women and Children's Medical Center, Guangzhou 510623, China, and Institut Pasteur de Shanghai, Chinese Academy of Sciences, Shanghai 200031, China. <sup>2</sup>The Center for Microbes, Development and Health, Key Laboratory of Molecular Virology and Immunology, Institut Pasteur de Shanghai, Chinese Academy of Sciences, Shanghai 200031, China. <sup>3</sup>University of Chinese Academy of Sciences, Shanghai 200031, China. <sup>4</sup>Program in Cellular and Molecular Medicine, Boston Children's Hospital, Boston, MA 02115, USA. <sup>5</sup>Department of Pediatrics, Harvard Medical School, Boston, MA 02115, USA. <sup>6</sup>Department of Biomedical Informatics, Harvard Medical School, Boston, MA 02115, USA. <sup>7</sup>Department of Dermatology and Harvard Skin Disease Research Center, Brigham and Women's Hospital, Harvard Medical School, Boston, MA 02115, USA. <sup>8</sup>Department of Medicine, Harvard Medical School, Boston, MA 02115, USA. \*Corresponding author. Email: judy.lieberman@childrens.harvard.edu (J.L.); xingliu@ips.ac.cn (X.L.) †These authors contributed equally to this work.

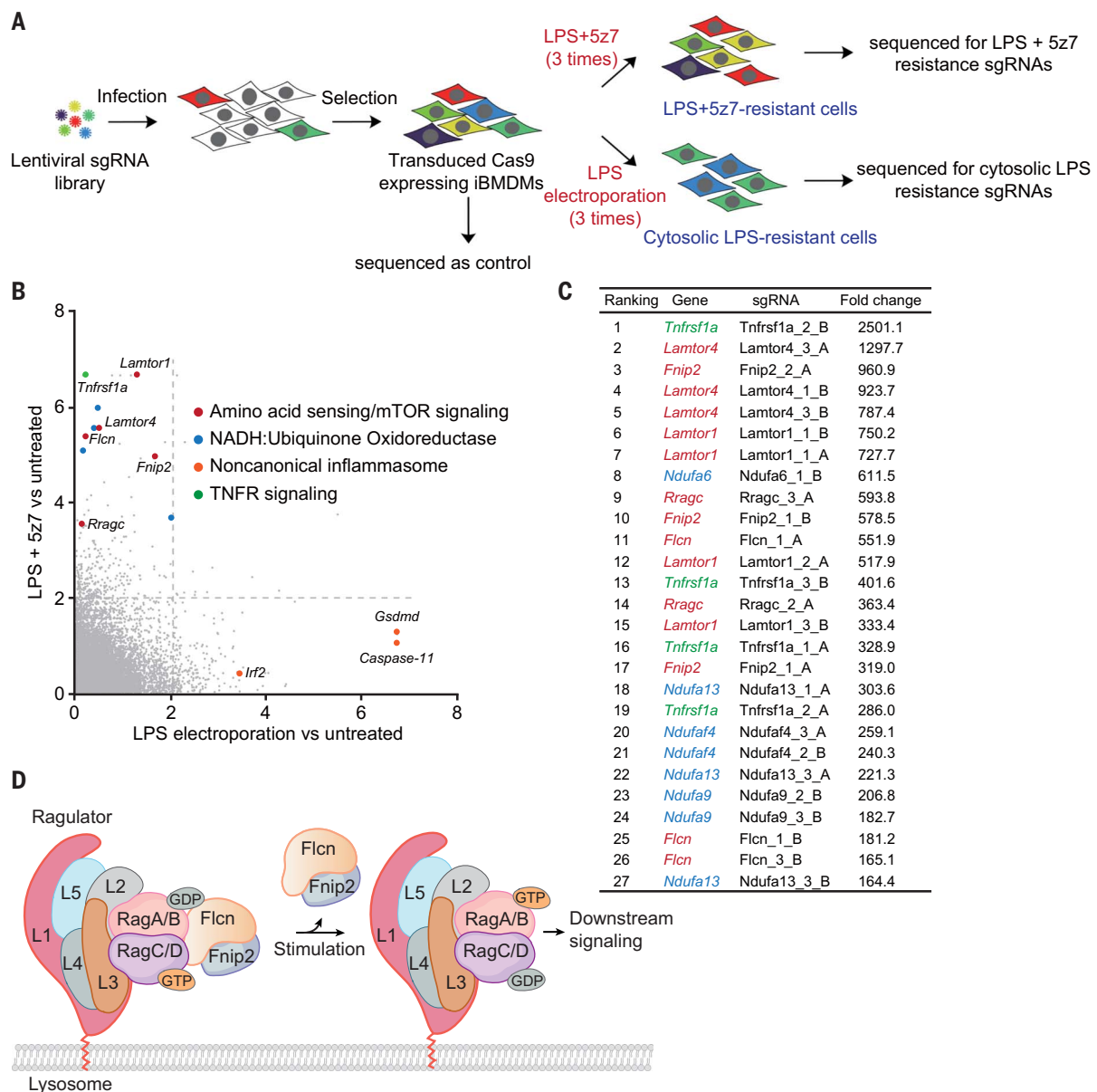


**Fig. 1. A genome-wide CRISPR screen identifies multiple components of the FLCN-FNIP2-Rag-Ragulator complex as needed for caspase-8-mediated pyroptosis.** (A) Schematic workflow of the genome-wide CRISPR screening procedure in iBMDMs. (B) -log<sub>10</sub>RR (robust rank aggregation) values calculated by the MAGeCK algorithm indicate the relative enrichment of genes after treatment with LPS electroporation (x axis) or LPS/5z7 (y axis) relative to controls in positive

selection. The dotted lines represent  $P = 0.01$ . (C) List of sgRNA hits from the screening in iBMDMs treated with LPS/5z7. Corresponding genes targeted with multiple sgRNAs and fold enrichments are shown. Green indicates genes encoding for the TNFR, red is the FLCN-FNIP2-Rag-Ragulator complex, and blue is the mitochondrial electron transport complex I. (D) Diagram of the FLCN-FNIP2-Rag-Ragulator complex.

RagB and GDP-loaded RagC or RagD); and FLCN complexed with its binding partners, Fnip1 or Fnip2 (FLCN-interacting protein 1/2), which facilitates the activation of the Rag heterodimer by catalyzing GTP hydrolysis of RagC or RagD (Fig. 1D). Because the identification of the lysosomal Rag-Ragulator complex was unexpected and dominated the list of most enriched sgRNAs, subsequent experiments focused on examining the putative role of Rag-Ragulator in caspase-8-mediated pyroptosis.

#### Ragulator complex is required for caspase-8-mediated, but not inflammasome-activated, pyroptosis

To verify the contribution of the Rag-Ragulator top gene hits to LPS/5z7-induced pyroptosis, we used CRISPR-Cas9-mediated gene editing to knock out *Lamtor1*, *Lamtor4*, *Rragc*, *Flcn*, and *Fnip2* in iBMDMs. For each gene, two clones transduced with distinct gRNAs that target different regions of each gene were obtained. Gene editing was verified by DNA

sequencing and immunoblot (Fig. 2A and fig. S2). Concurrent treatment of wild-type (WT) iBMDMs with LPS and 5z7 resulted in rapid pyroptotic cell death, as assessed by lactate dehydrogenase (LDH) release, but iBMDMs deficient in each of the Rag-Ragulator genes tested were highly resistant to LPS/5z7-induced pyroptosis (Fig. 2A and fig. S3A). Consistent with the dependency of caspase-8-mediated pyroptosis on these genes, caspase-8 maturation and GSDMD cleavage to the p30 and p20

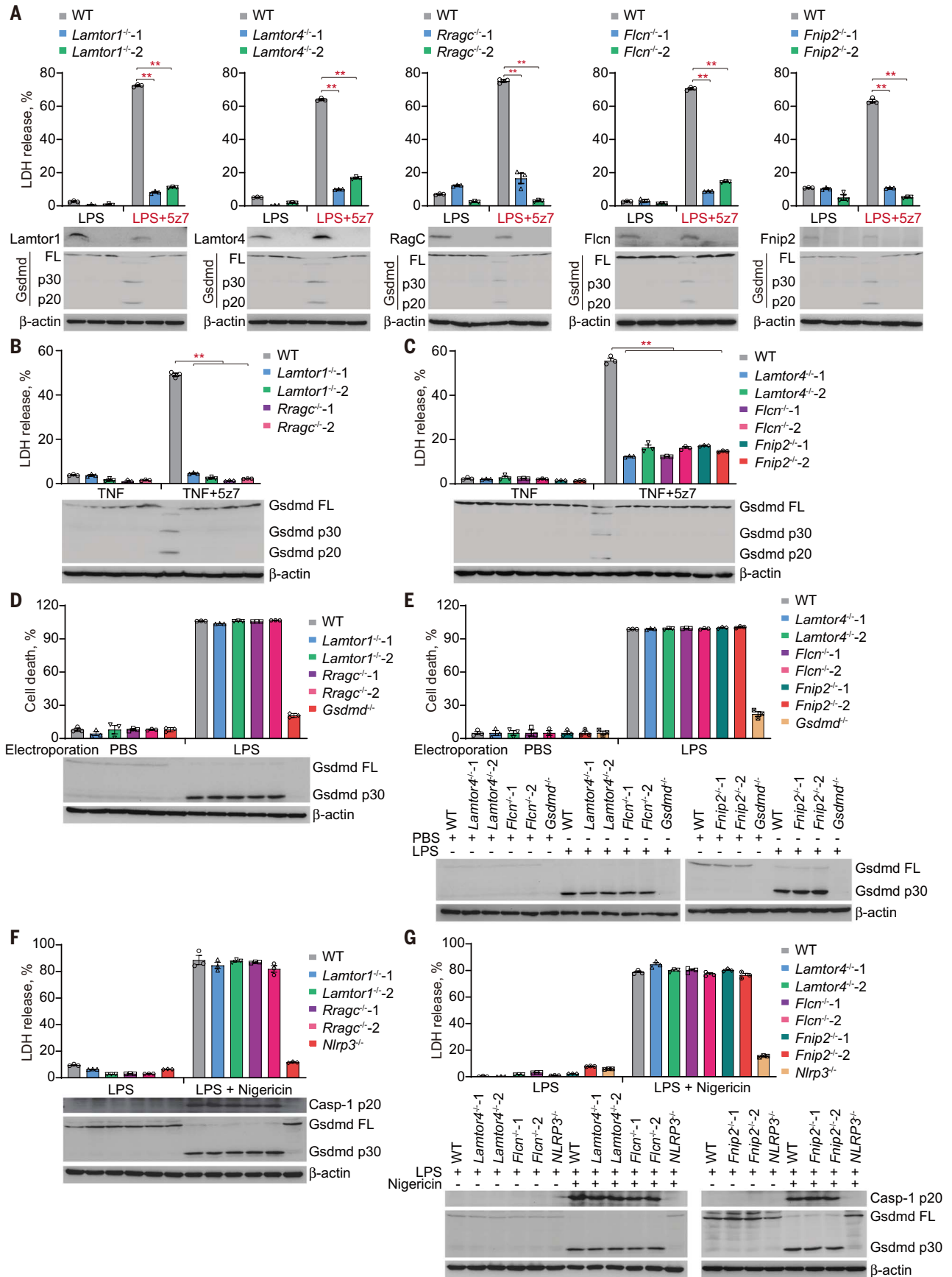


## Fig. 2. FLCN–FNIP2–Rag–Ragulator gene deficient cells are resistant to LPS/5z7 treatment but sensitive to inflammasome-induced pyroptosis.

(A) The indicated iBMDMs were challenged with LPS or LPS/5z7. Cell death was measured by LDH release after 2.5 hours. Specific gene ablation was confirmed and Gsdmd cleavage was examined by immunoblot, as shown in the bottom panel. (B, C, F, and G) The indicated iBMDMs were treated with TNF- $\alpha$  (abbreviated to TNF in the figure), TNF- $\alpha$ /5z7 [(B) and (C)], or LPS/nigericin [(F) and (G)].

fragments, which were detected by immunoblot in LPS- and 5z7-treated WT iBMDMs, were not detected in the knockout cells (Fig. 2A and fig. S3B). iBMDMs knocked out for the same set of Rag–Ragulator genes also survived treatment with an alternate stimulus of caspase-8–dependent pyroptosis (TNF- $\alpha$  plus 5z7) (12) and showed no sign of GSDMD cleavage (Fig. 2, B and C). Caspase-3/7 cleavage, occurring downstream of caspase-8 activation (13, 23), was blunted by Rag–Ragulator deficiency upon LPS/5z7 treatment (fig. S3B). By contrast, Rag–Ragulator deficiency had no effect on caspase-3/7 cleavage or activation in etoposide-induced apoptosis (fig. S3C), indicating the specific role of Rag–Ragulator in LPS/5z7-induced pyroptosis. To determine whether the Rag–Ragulator complex was also involved in inflammasome and inflammatory caspase–mediated pyroptosis, WT and knockout clones of iBMDMs were treated with two stimuli of canonical inflammasomes and caspase-1-mediated pyroptosis [LPS plus nigericin to activate the NLRP3 inflammasome or anthrax-protective antigen (PA) plus lethal factor-flagellin fusion protein (LFN-Fla) to activate the NLRC4 inflammasome] or were electroporated with LPS to induce the noncanonical caspase-11 inflammasome and pyroptosis (Fig. 2, D to G, and fig. S4). WT iBMDMs and iBMDMs knocked out for the five Rag–Ragulator genes were all similarly killed by activating the canonical or noncanonical inflammasomes. As positive controls and as expected, iBMDMs genetically deficient in *Gsdmd* were resistant to electroporated LPS, iBMDMs deficient in *Nlrp3* were resistant to LPS plus nigericin, and iBMDMs deficient in *Nlr4* were resistant to PA plus LFN-Fla. In these experiments cell death was assessed either by an ATP assay measuring surviving cells or an LDH assay measuring pyroptosis. GSDMD cleavage, assessed by immunoblot, correlated with cell death, as expected. Thus, *Lamtor1*, *Lamtor4*, *Rragc*, *Flcn*, and *Fnip2* are selectively required for RIPK1–caspase-8–dependent pyroptosis but not for inflammasome-mediated pyroptosis.

### The Rag–Ragulator complex recruits RIPK1 and caspase-8 to the lysosomal membrane

Because the Rag–Ragulator complex is localized to the lysosomal membrane and is required for caspase-8–mediated pyroptosis, we postulated that RIPK1 and caspase-8 might be recruited to and activated on the lysosomal membrane after LPS/5z7 treatment. In the absence of cFLIP<sub>L</sub>,

TLR4 signaling typically causes the assembly of a complex containing a death domain–containing protein FADD and RIPK1 that recruits and activates caspase-8 (24). The complex also assembles in response to LPS/5z7 (24). Consistently, within 100 min of adding LPS/5z7, but not LPS on its own, FADD immunoprecipitated with RIPK1, procaspase-8, and the p43 subunit of activated caspase-8, indicating the formation of a FADD–RIPK1–caspase-8–containing complex that activated caspase-8 (Fig. 3A). Although cleaved caspase-8 levels increased by 150 min, the RIPK1 band was strongly diminished and the interaction of FADD with both RIPK1 and caspase-8 became undetectable, suggesting that the complex was transient and disintegrated, potentially because of RIPK1 degradation. To determine whether the complex depended on Rag–Ragulator, the experiment was repeated in iBMDMs knocked out for *Rragc*. In RagC-deficient cells treated with LPS/5z7, FADD did not pull down RIPK1 or caspase-8, RIPK1 was not degraded, and the p43-activated caspase-8 band was barely detected (Fig. 3A). These data suggest that assembly of the FADD–RIPK1–caspase-8 complex depends on Rag–Ragulator and might be recruited to lysosomes for subsequent function. Indeed, treatment with LPS/5z7 significantly and specifically induced colocalization of caspase-8 and RIPK1 with lysosomes, but not endoplasmic reticulum, mitochondria, or early endosomes, and was dependent on Lamtor1 (Fig. 3, B to D, and fig. S5). To confirm that RIPK1 and caspase-8 colocalize with Rag–Ragulator after LPS/5z7 stimulation, hemagglutinin (HA)–tagged RIPK1 (Fig. 3E) and caspase-8 (Fig. 3F) were coexpressed with Flag-tagged Lamtor1, RagC, Flcn, or Fnip2 in human embryonic kidney (HEK) 293T cells, and coimmunoprecipitation was assessed by anti-HA immunoprecipitation followed by anti-Flag immunoblot. Coimmunoprecipitation of both RIPK1 and caspase-8 with RagC and Flcn was detected but not with Lamtor1 or Fnip2 (Fig. 3, E and F). Moreover, interaction of endogenous RIPK1 and caspase-8 with RagC could both be detected in iBMDMs treated with LPS/5z7 (Fig. 3G). Compared with GTP-loaded inactive RagC (Q119L), GDP-loaded active RagC (S74N) showed stronger binding to RIPK1/caspase-8 (Fig. 3, H and I). Mapping of interactive domains by truncation revealed that the kinase domain (KD) of RIPK1 and the caspase domain (CD) of caspase-8 were required and sufficient for RagC binding (fig. S6).

and (G)]. Cell death was measured by LDH release after 2.5 hours [(B) and (C)] or 1.5 hours [(F) and (G)]. (D and E) The indicated iBMDMs were electroporated with LPS. Cell death was assessed and calculated by measuring the ATP level after 2.5 hours. Gsdmd cleavage and caspase-1 processing (during canonical inflammasome activation) were examined by immunoblot. Graphs show mean  $\pm$  SEM of triplicate wells. Data are representative of at least three independent experiments. Data were analyzed using a two-tailed Student's *t* test. \*\*\**P* < 0.01.

These domains are distinct from the domains implicated in RIPK1 binding to caspase-8 and FADD through a death domain (DD)–death effector domain (DED) interaction and DD–DD interaction, respectively (25–27), and in caspase-8 binding to FADD through a DED–DED interaction (28, 29). Because caspase-8–mediated pyroptosis depended on Lamtor1 and Fnip2, we suspect that RIPK1 and caspase-8 associate with the large supercomplex, but their interaction with these other components could be indirect. This result suggested that RIPK1 and caspase-8 directly interacted with RagC and Flcn, which are in contact with each other in the cryo–electron microscopy structure of the human Rag–Ragulator supercomplex (30). Thus, Rag–Ragulator acts as a lysosomal platform for recruiting RIPK1 and procaspase-8 and activating caspase-8.

### Neither mTOR activity nor Tfeb/Tfe3 is involved in caspase-8– or inflammasome-induced pyroptosis

Because the Rag–Ragulator complex regulates mTORC1 activation, we next investigated whether caspase-8–mediated pyroptosis is regulated by mTORC1. To inhibit mTORC1, iBMDMs were treated with rapamycin, a potent allosteric mTORC1 inhibitor, or with Torin 1, a selective ATP-competitive mTORC1/2 inhibitor (31). Both inhibited mTORC1 kinase activity in iBMDMs at the doses used and caused dephosphorylation of the mTORC1 target p70 S6 kinase (fig. S7A). However, incubation of iBMDMs with rapamycin or Torin 1 before treatment with LPS/5z7 had no effect on GSDMD cleavage or on the extent or kinetics of pyroptotic cell death, as assessed by propidium iodide (PI) uptake (Fig. 4, A and B). Furthermore, treatment with 5-aminoimidazole-4-carboxamide riboside (AICAR), which blocks mTOR signaling by activating AMP-activated protein kinase (AMPK), did not affect LPS/5z7-triggered GSDMD cleavage or pyroptosis (Fig. 4C and fig. S7B). Thus, mTOR kinase activity does not affect caspase-8–induced pyroptosis, although the Rag–Ragulator complex is required. These mTORC1 inhibitors also did not affect electroporated LPS-induced noncanonical inflammasome or LPS plus nigericin-induced canonical inflammasome activation of GSDMD cleavage or pyroptosis (Fig. 4, D and E). Thus, mTOR activity is not involved in pyroptosis triggered by TAK1 inhibition or inflammasome signaling. In addition, simultaneous knockdown

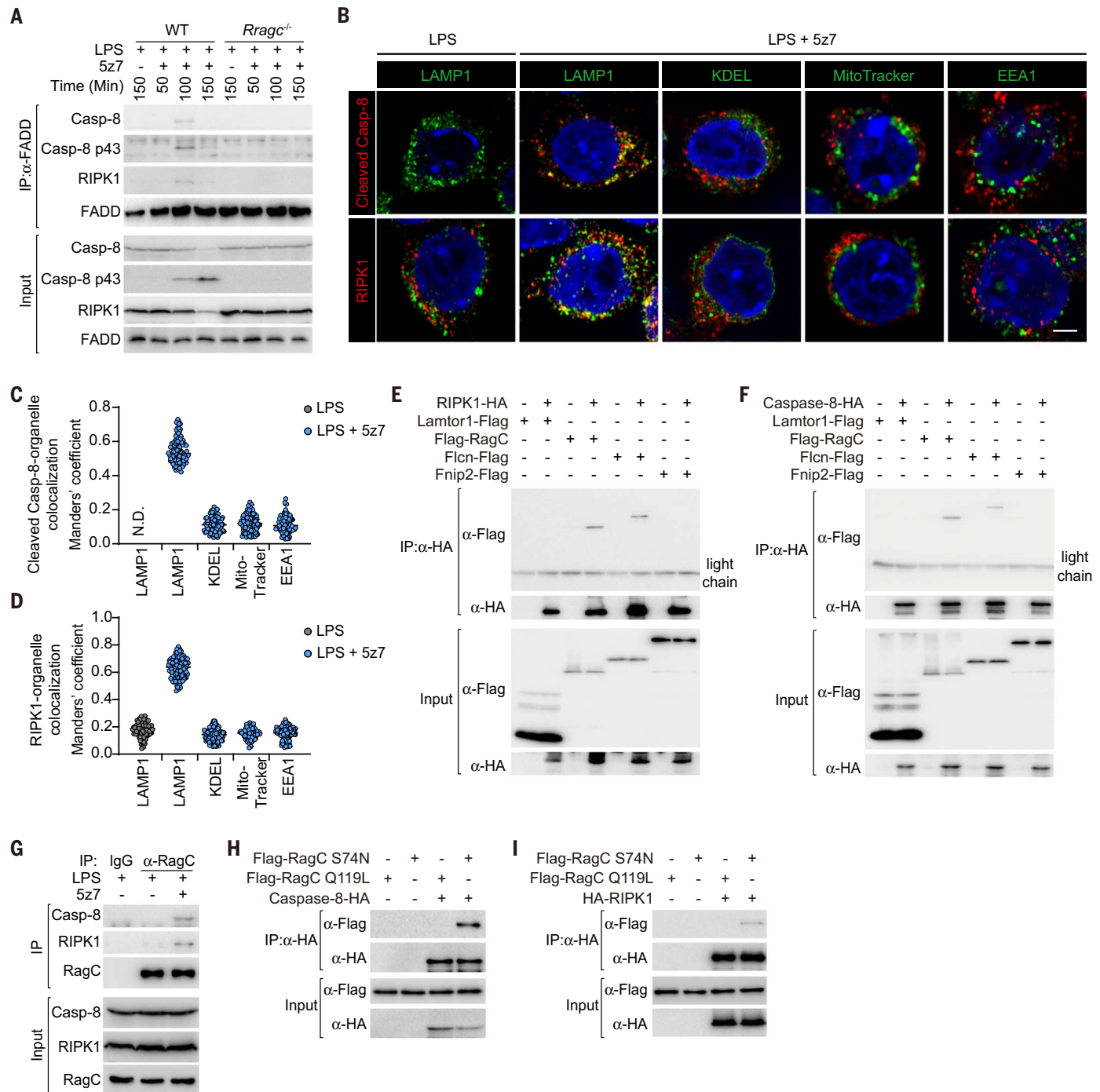


**Fig. 3. Recruitment and activation of an LPS/5z7-induced FADD–RIPK1–caspase-8 complex to lysosomes depends on binding to RagC and Flcn in the Rag-Ragulator complex.** (A) WT and *Rragc*<sup>-/-</sup> iBMDMs were treated with LPS/5z7 for the indicated times. Endogenous FADD complex was immunoprecipitated with anti-FADD antibody and analyzed by immunoblot with the indicated antibodies. (B) Representative confocal fluorescence images of LPS or LPS plus 5z7-treated iBMDMs co-stained for cleaved caspase-8 or RIPK1 with the indicated organelle markers (LAMP1, lysosomes; KDEL, endoplasmic reticulum; MitoTracker, mitochondria; EEA1, early endosomes) and DAPI. Scale bars, 2  $\mu$ m. (C and D) Quantification

of colocalization of cleaved caspase-8 (C) and RIPK1 (D) with organelles in multiple confocal images [as in (B)] by calculating Manders' overlap coefficient (each point represents a single cell). N.D., not detected. (E, F, H, and I) Lysates of HEK293T cells transfected with the indicated plasmids were assayed for immunoprecipitation with anti-HA antibody and analyzed by immunoblot probed with the indicated antibodies. (G) Lysates of iBMDMs treated with LPS or LPS/5z7 were assayed for immunoprecipitation with anti-RagC antibody and analyzed by immunoblot probed with the indicated antibodies. Data are representative of at least three independent experiments.

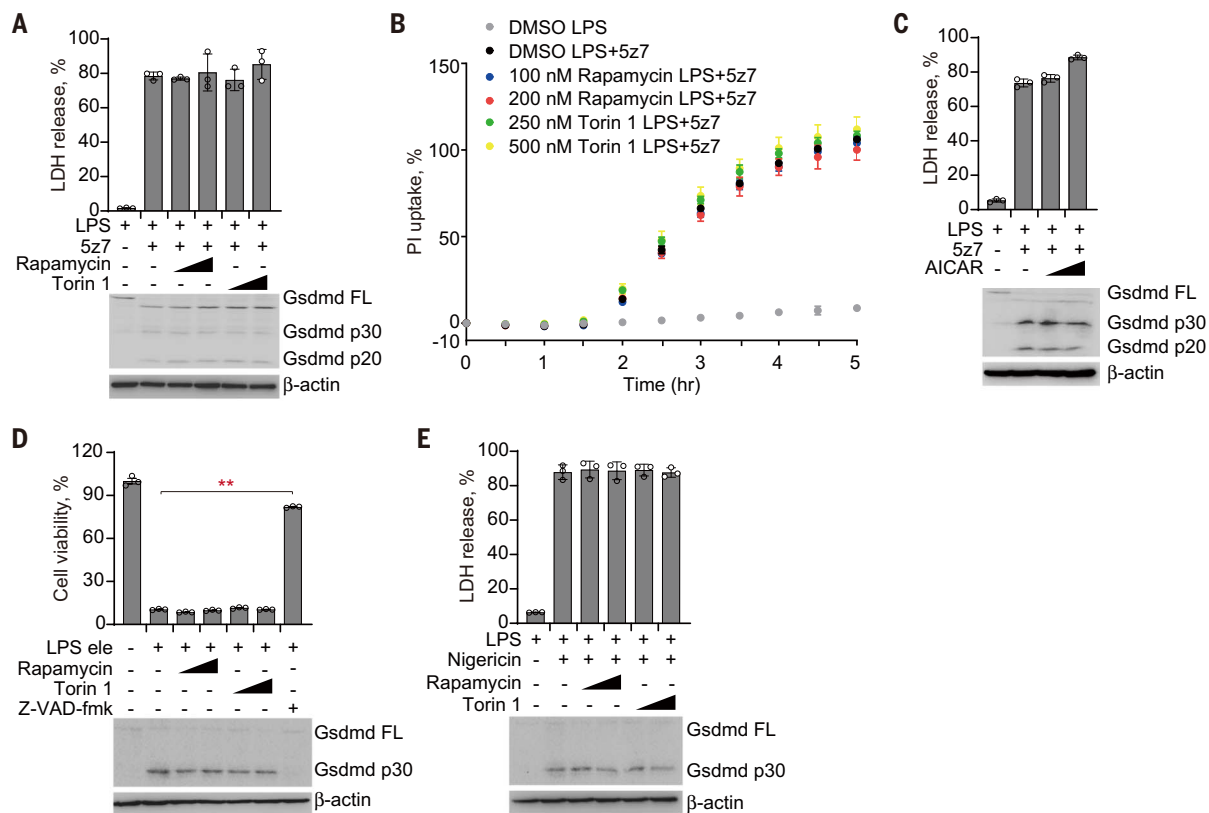


**Fig. 4. mTORC1 activity is not required for LPS/5z7- or inflammasome-triggered pyroptosis.** (A and B) iBMDMs preincubated with rapamycin or Torin 1 for 2 hours were treated with LPS or LPS/5z7, and cell death was measured by LDH release after 2.5 hours (A) or by entry of PI into cells (B). (C) iBMDMs preincubated with AICAR for 2 hours were treated with LPS or LPS/5z7, and cell death was measured by LDH release 2.5 hours later. (D) iBMDMs preincubated with rapamycin or Torin 1 for 2 hours were

electroporated (ele) with LPS, and cell viability was assessed by measuring the ATP level 2.5 hours later. (E) iBMDMs preincubated with rapamycin or Torin 1 for 2 hours were treated with LPS or LPS/nigericin, and cell death was measured by LDH release 1.5 hours later. Gsdmd cleavage was examined by immunoblot. Graphs show mean  $\pm$  SEM of triplicate wells. Data are representative of at least three independent experiments. Data were analyzed using a two-tailed Student's *t* test. **\*\****P* < 0.01.

of the MiT/TFE family transcription factors Tfeb and Tfe3, master regulators of lysosomal biogenesis and autophagy in response to various stresses, showed no effect on LPS/5z7-triggered pyroptosis of Ragulator/Rag/Fcn-deficient cells (fig. S8, A to D). Forced nuclear localization and activation of Tfeb (S14I, 210A) also did not affect LPS/5z7-induced pyroptosis (fig. S8, E and F), ruling out the possibility that the defects of Fcn-Rag-Ragulator-knockout cells in LPS/5z7-triggered pyroptosis resulted from constitutive nuclear localization of Tfeb/Tfe3 and subsequent induction of downstream autophagy-lysosomal gene expression (32, 33).

#### Lysosomal tethering of Ragulator is required for TAK1 inhibition-induced pyroptosis

We next investigated whether lysosomal localization of Rag-Ragulator is required for TAK1 inhibition-induced pyroptosis. Rag-Ragulator is tethered to the cytosolic side of the lysosomal membrane by lipidation of Lamtor1 at its N-terminal G2 and C3C4 residues (21, 22). To address this question, we ectopically expressed WT or a *Lamtor1* mutant of its three

N-terminal lipidation sites to alanine (*Lamtor1* 3A) in *Lamtor1*<sup>-/-</sup> iBMDMs. *Lamtor1* 3A was no longer tethered to the lysosome and re-distributed to the cytosol (Fig. 5A). Rescue of *Lamtor1*<sup>-/-</sup> by ectopic expression of WT *Lamtor1* in iBMDMs restored LPS/5z7-induced pyroptosis, as assessed by measuring LDH release, PI uptake, and pyroptotic morphological changes (ballooning cell membrane) (Fig. 5, B to D). By contrast, *Lamtor1* 3A did not rescue LPS/5z7-induced pyroptosis, indicating that Ragulator needs to be tethered to the lysosome to promote LPS/5z7-induced pyroptosis. Overexpression of *Lamtor1* 3A disrupted the cleavage and lysosomal localization of caspase-8 after LPS/5z7 treatment (fig. S9). Next, we used immunoblotting to determine which step in RIPK1-caspase-8-GSDM-mediated pyroptosis was regulated by Ragulator (Fig. 5E). In WT iBMDMs, phosphorylation of RIPK1 at Ser166 was detected within 100 min of adding LPS/5z7, which was followed by detection of RIPK1 cleavage and cleavage of caspase-8 and GSDMD to their active fragments at 150 min. GSDME was also cleaved concurrently to produce

a p30 active N-terminal fragment. The detection of activated caspase-8, GSDMD, and GSDME fragments coincided with the kinetics of membrane disruption recorded by PI uptake in WT iBMDMs (Fig. 5C). By contrast, *Lamtor1*-deficient iBMDMs showed severely blunted RIPK1 phosphorylation and cleavage and caspase-8, GSDMD, and GSDME activation (Fig. 5E). Reexpression of *Lamtor1* restored the defects in RIPK1 and caspase-8 activation as well as GSDM cleavage in *Lamtor1*-deficient cells. Thus, the activation of RIPK1 and the downstream caspase-8-GSDM pyroptotic pathway only occurs when the RIPK1-caspase-8-containing complex is anchored to the lysosomal membrane by Ragulator.

Next, we examined the role of lysosomal Ragulator in pyroptosis induced by *Y. pseudotuberculosis*. Like LPS/5z7 treatment, *Yersinia* infection in WT iBMDMs triggered massive pyroptosis, as assessed by LDH release, which, as expected, was associated with caspase-8 and GSDMD cleavage to their active forms (Fig. 5F). For the first 60 min after infection, before pyroptosis occurred, bacterial replication as

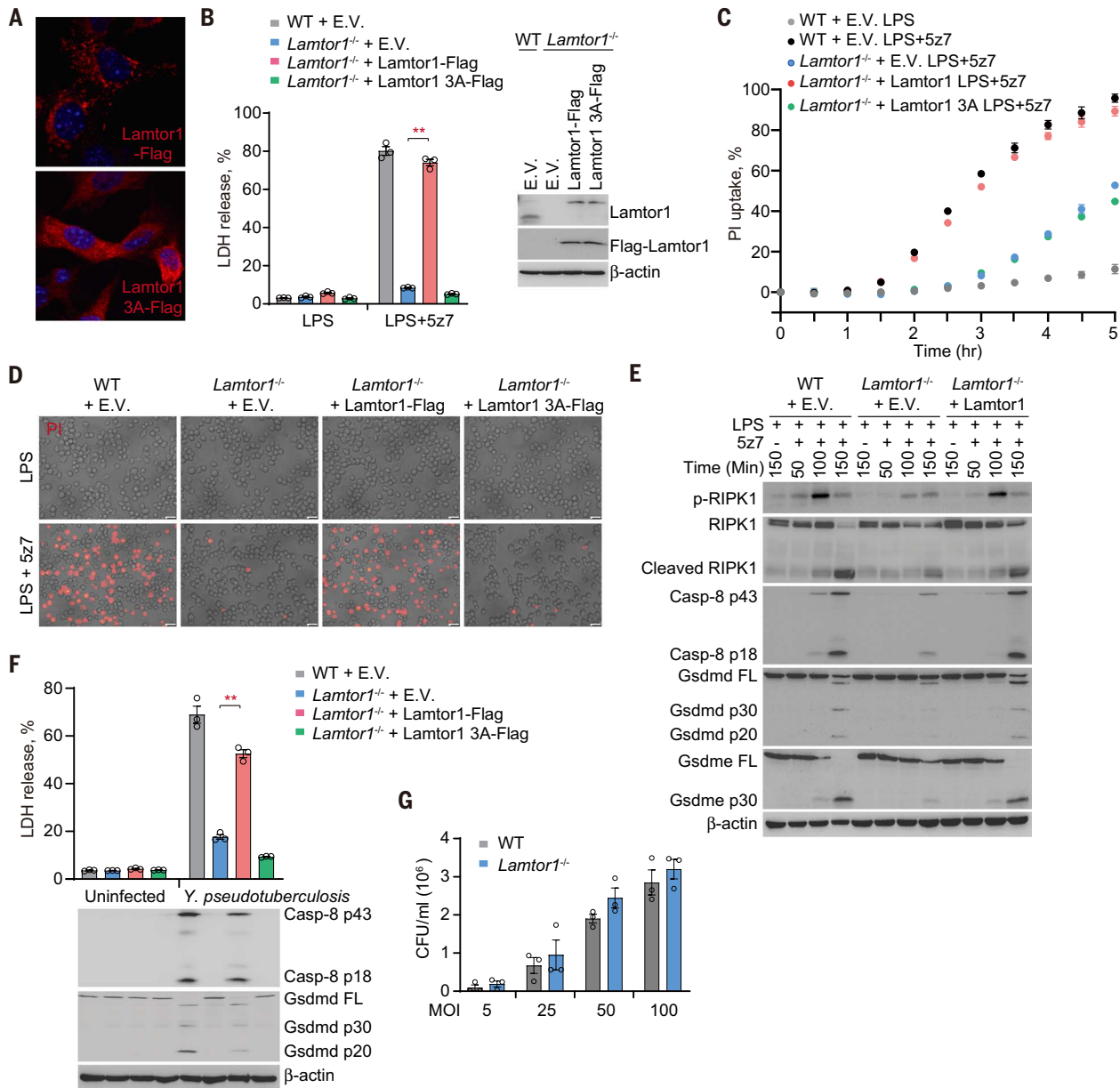


**Fig. 5. Pyroptosis activated by LPS/5z7 or pathogenic *Yersinia* depends on lipidated Lamtor1.** (A) The subcellular localization of Lamtor1 and Lamtor1 3A mutant was imaged by confocal microscopy. (B, C, D, and F) The indicated iBMDMs were treated with LPS, LPS/5z7 [(B) to (D)], or *Yersinia* (F). Cell death was measured by LDH release after 2.5 hours (B) or after 5 hours (F), by the entry of PI into cells in real time (C), or as observed by phase-contrast fluorescence microscopy (D). (E) Full-length and cleaved products of caspase-8,

RIPK1, Gsdmd, and Gsdme from whole-cell lysates of the indicated iBMDMs treated with LPS or LPS/5z7 for the indicated times. (G) The amount of *Yersinia* taken up by WT or *Lamtor1*<sup>-/-</sup> iBMDMs was quantified by counting colony-forming units (CFUs). Graphs in (B), (C), (F), and (G) show mean  $\pm$  SEM of triplicate wells. Data are representative of at least three independent experiments. Data were analyzed using a two-tailed Student's *t* test. \*\**P* < 0.01. E.V., empty vector.

measured by colony counts was comparable in WT and *Lamtor1*<sup>-/-</sup> iBMDMs (Fig. 5G). Lamtor1 deficiency also did not affect the secretion and activity of YopJ (fig. S10). However, cell death and caspase-8 and GSDMD processing were strongly reduced in *Lamtor1*<sup>-/-</sup> iBMDMs (Fig. 5F). Pyroptosis was rescued by ectopic expression of Flag-tagged WT Lamtor1 but not Lamtor1 3A. Thus, lysosomal targeting of Lamtor1 is also a prerequisite for *Yersinia*-triggered pyroptosis.

#### Lysosomal Rag GTPase drives RIPK1-caspase-8-induced pyroptosis

Our genetic screen and its validation (Figs. 1 and 2) suggested that RagC and Flcn-Fnip, which activates RagC's GTPase activity by converting RagC into the GDP-loaded form (22, 34, 35), were required for RIPK1-caspase-8-mediated pyroptosis. To determine which form of RagC promotes TAK1 inhibition-triggered pyroptosis, we reintroduced RagC

WT, the GTP-bound form of RagC (RagC Q119L), or the GDP-bound form of RagC (RagC S74N) into RagC-deficient iBMDMs. Ectopic expression of either RagC WT or the GDP-bound form of RagC restored LPS/5z7-mediated pyroptosis to *Rragc*-knockout iBMDMs, as assessed by LDH release, PI uptake, and ballooning morphology, whereas the GTP-bound form of RagC failed to do so (Fig. 6, A to C). RagC deficiency inhibited activation of RIPK1, caspase-8, GSDMD, and

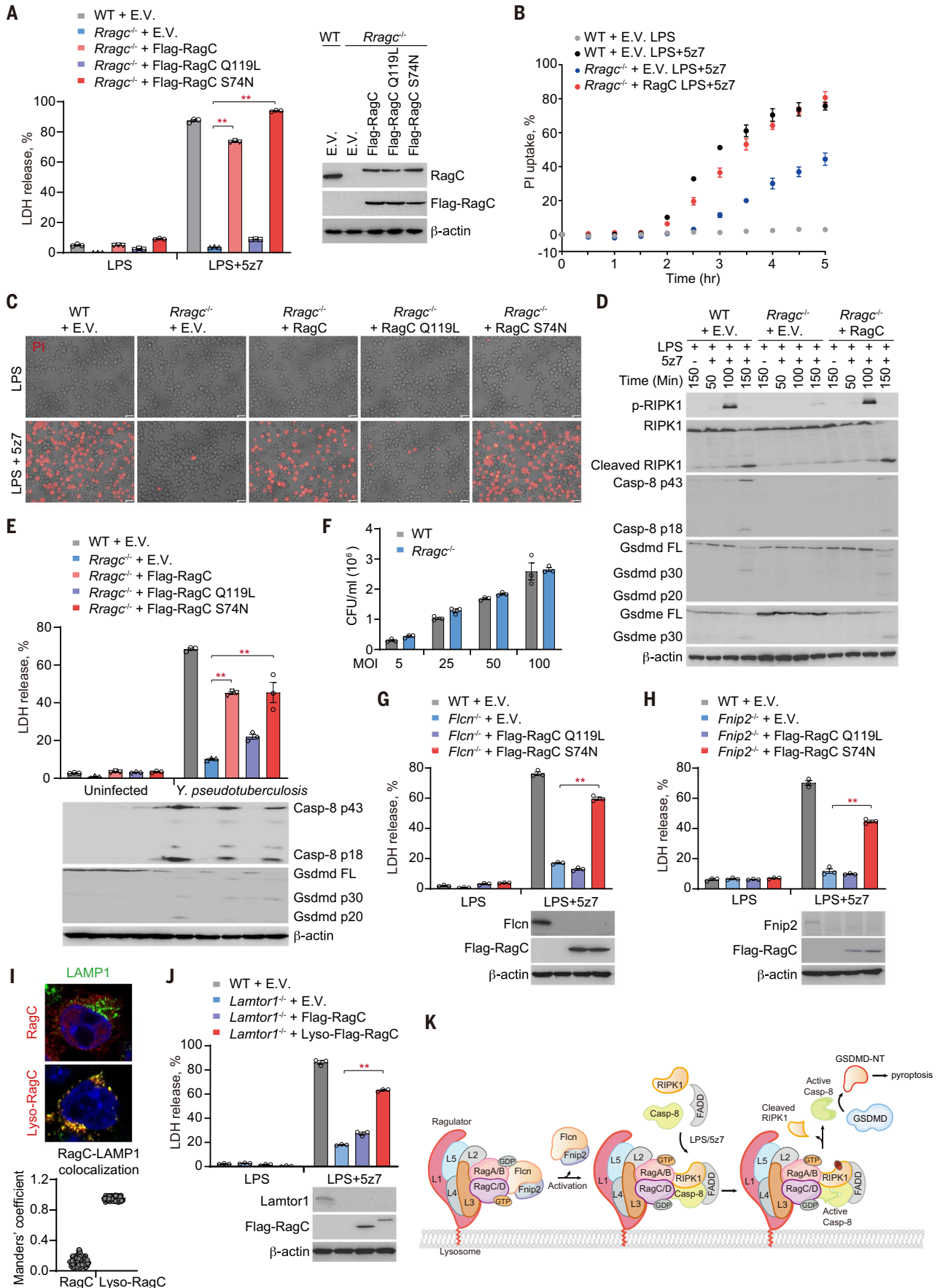


**Fig. 6. GTPase activity of lysosomal membrane-anchored RagC is required for caspase-8 activation and pyroptosis triggered by LPS/5z7 or pathogenic *Yersinia*.** (A, B, C, and E) The indicated iBMDMs were treated with LPS, LPS/5z7, or *Yersinia*. Cell death was measured by LDH release after 2.5 hours (A) or 5 hours (E), by the entry of PI into cells in real time (B), or as observed by phase-contrast fluorescence microscopy (C). (D) Full-length and cleaved products of caspase-8, RIPK1, Gsdmd, and Gsdme from whole-cell lysates of the indicated iBMDMs treated with LPS or LPS/5z7 for the indicated times. (F) The amount of *Yersinia* taken up by WT or *Rragc*<sup>-/-</sup> iBMDMs was quantified by counting CFUs. (G, H, and J) WT,

*Flcn*<sup>-/-</sup>, *Fnip2*<sup>-/-</sup>, or *Lamtor1*<sup>-/-</sup> iBMDMs reintroduced with the indicated plasmids were treated with LPS/5z7 and assayed for LDH release 2.5 hours later. (I) Lysosomal localization of ectopically expressed RagC and Lyso-RagC in *Lamtor1*<sup>-/-</sup> iBMDMs was assessed by confocal microscopy (representative images, upper panel). Colocalization of RagC with LAMP1 was analyzed by calculating Manders' overlap coefficient (lower panel). (K) Model of RIPK1-caspase-8 activation mediated by Rag-Ragulator complex. Graphs in (A), (B), (E) to (H), and (J) show mean ± SEM of triplicate wells. Data are representative of at least three independent experiments. Data were analyzed using a two-tailed Student's *t* test. \*\**P* < 0.01.

GSDME, which could be rescued by reexpression of RagC (Fig. 6D). Similarly, ectopic expression of WT or GDP-bound RagC in RagC-deficient iBMDMs made them susceptible to pyroptosis caused by infection of pathogenic *Yersinia*, whereas the GTP-bound form of RagC did not (Fig. 6E). The presence of RagC did not affect bacterial replication at early time points or the secretion and activity of YopJ (Fig. 6F and fig. S10). By comparison, *Salmonella* infection-induced, caspase-1-dependent GSDMD cleavage and pyroptosis in iBMDMs were not affected by *Rragc* knockout or knockout of any of the other Rag-Ragulator complex genes tested (*Lamtor1*, *Lamtor4*, *Flcn*, and *Fnip2*) (fig. S11). Thus, the GDP-bound form of RagC selectively mediates caspase-8-induced pyroptosis. We hypothesized that Ragulator and Flcn-Fnip function upstream of the Rag GTPase to tether it to the lysosome and maintain it in its GDP-bound state. To test this hypothesis, we performed rescue experiments in *Flcn*- or *Fnip2*-deficient iBMDMs by reintroducing RagC (Fig. 6, G and H). Ectopic expression of GDP-bound RagC restored susceptibility of *Flcn*- or *Fnip2*-deficient iBMDMs to LPS/5z7-triggered pyroptosis, whereas the GTP-bound form of RagC did not. To determine whether Ragulator's role was primarily to direct RagC to the lysosomal membrane, we generated a RagC construct in which the lysosomal targeting sequence of *Lamtor1* was added to the N terminus of RagC (called Lyso-RagC). Although lysosomal localization of WT RagC was lost in *Lamtor1*-deficient cells, the lysosomal targeting sequence relocalized Lyso-RagC to the lysosome when *Lamtor1* was lacking (Fig. 6I). Ectopic expression of Lyso-RagC made *Lamtor1*-deficient cells sensitive to LPS/5z7-triggered pyroptosis (Fig. 6J). In addition, LPS/5z7 treatment did not affect the subcellular localization of *Flcn* (fig. S12). Thus, lysosomal targeting of GDP-bound RagC is sufficient to trigger caspase-8-mediated pyroptosis.

## Discussion

Recent studies revealed an alternative inflammasome- and inflammatory caspase-independent, but caspase-8- and gasdermin-dependent, pyroptotic pathway activated by TLR/TNF- $\alpha$  signaling during pathogenic *Yersinia* infection (12, 13). Here, in an unbiased CRISPR

screen, we discovered a critical and unexpected role of the lysosomal membrane-tethered Rag-Ragulator supercomplex. Rag-Ragulator served as a platform for activating a FADD-RIPK1-caspase-8 complex formed in response to TLR/TNFR ligation, and Rag GTPase activity was critical for triggering the pathway (Fig. 6K). There is still much to learn. Future kinetics, biochemistry, and live-cell imaging experiments can determine whether the FADD-RIPK1-containing complex recruits caspase-8 before or after Rag-Ragulator binding and whether it contains other components or if its formation is regulated by posttranslational modifications of its component proteins. Our data suggest that the death-receptor-triggered complex binds to RagC and *Flcn*, but does the Rag-Ragulator complex remain intact after binding or do some components dissociate? Are other proteins recruited? Although we found that mTORC1 activity did not affect caspase-8 activation or pyroptosis, does the FADD-RIPK1-caspase-8 complex compete for binding to Rag-Ragulator with mTORC1? Does cellular metabolism (amino acid and ATP availability and cellular stress, which regulate mTORC1), affect the execution of this cell death pathway? One study suggests that lysosomes are disrupted during inflammasome-mediated pyroptosis (36). Do the gasdermins form pores in lysosomal membranes to disrupt lysosomes and cause their proteases to be released into the cytosol and wreak additional damage? RIPK1 phosphorylation is Rag dependent and occurs once the complex is bound to Rag-Ragulator. Activated caspase-8 cleaved and activated both GSDMD and GSDME, as has been shown previously (12, 13), but the mechanism for GSDME cleavage is uncertain. Does caspase-8 directly cleave GSDME or is cleavage indirect through caspase-8 cleavage of caspase-3, a known activator of GSDME? The role of Rag-Ragulator in pyroptosis described here confirms the key role of Rag-Ragulator as a central hub for monitoring environmental cues. This role is now extended to include infection as well as nutrient and energy availability and helping to decide not only whether a cell proliferates but also whether it survives. Future studies can leverage these insights to explore more mechanistic details of pyroptosis, as well as to manipulate this process for therapeutic benefits.

## Materials and methods

### Plasmids, antibodies, and reagents

psPAX2 (#12260), pMD2.G (#12259), lentiCas9-Blast (#52962), lentiCRISPR v2 (#52961), pFastBacDual with LFn + Fla (#84866), and pFastBacDual with PA+His tag (#84870) constructs were obtained from Addgene. Mouse *Ripk1*, *Casp-8*, *Lamtor1*, *Rragc*, *Flcn*, *Fnip2*, and *Tfeb* were amplified by polymerase chain reaction (PCR) from the mouse cDNA library and cloned into mammalian expression vectors (pHAGE-BSD-Flag, pHAGE-Ble, pcDNA3-NHA, or pcDNA3-CHA). All point mutations and truncations were generated using the overlap PCR method. For short hairpin RNA (shRNA) cloning, annealed shRNA oligos were ligated into pLKO.1 (Addgene #8453). The oligo sequences for targeting the genes of interest were as follows: negative control (5'-CCT AAG GTT AAG TCG CCC TCG-3'), *Tfeb* (5'-GCA GGC TGT CAT GCA TTA TAT-3'), and *Tfeb3* (5'-GCC TAA CAT CAA ACG CGA GAT-3'). All plasmids were verified by sequencing.

Monoclonal anti-Flag antibody (F3165) and anti- $\beta$ -actin antibody (A1978) were from Sigma-Aldrich. Antibodies against HA (#3724, #2367), Flag (#14793), TFEB (#32361), TFE3 (#14779), EEA1 (#48453), p70 S6 Kinase (#2708), Phospho-p70 S6 Kinase (#9234), p38 (#9212), Phospho-p38 (#4511), Erk (#4695), Phospho-Erk (#4370), cleaved caspase-8 (#8592), caspase-8 (#4927), caspase-3 (#9665), caspase-7 (#12827), RIPK1 (#3493), Phospho-RIPK1 (#31122), RagC (#3360, #9480), *Lamtor1* (#8975), *Lamtor4* (#12284), and *FLCN* (#3697) were from Cell Signaling Technology. Monoclonal anti-FADD antibody (sc-166516) and monoclonal anti-KDEL antibody (sc-58774) were from Santa Cruz Biotechnology. Monoclonal anti-LAMP1 antibody was from Developmental Studies Hybridoma Bank (1D4B). Monoclonal anti-GSDMD antibody (ab209845), monoclonal anti-GSDME antibody (ab215191), polyclonal anti-FNIP2 antibody (ab106611), monoclonal anti-pro caspase-8 antibody (ab108333), monoclonal anti-LAMP1 antibody (ab208943), and monoclonal anti-FADD antibody (ab124812) were from Abcam. Anti-YopJ antibody was kindly shared by Professor Zongmin Du (Beijing Institute of Microbiology and Epidemiology, China).

LPS (#L4524), etoposide (#E1383), polybrene (#H9268), rapamycin (#V900930), 5z7 (O9890),

and AICAR (#A9978) were from Sigma-Aldrich. Recombinant murine TNF- $\alpha$  (#315-01A) was from Peprotech. Z-VAD-fmk (#550377) was from BD Pharmingen. Ultrapure LPS (tlrl-3pelps), nigericin (tlrl-nig), and blasticidin (anti-bl) were from Invivogen. Torin 1 (#MB3467) was from Meilunbio. Puromycin (#A1113802), zeocin (#R25005), and MitoTracker (#M7510) were from Invitrogen.

#### Cell culture and stimulation

HEK293T, mouse embryonic fibroblasts, and C57BL/6 mouse iBMDM cells, described previously (7), were cultured in Dulbecco's modified Eagle's medium supplemented with 10% fetal bovine serum, 1 $\times$  GlutaMAX (ThermoFisher, #35050061), 1 $\times$  penicillin-streptomycin (ThermoFisher Scientific, #15140148), and 50  $\mu$ M 2-Mercaptoethanol ( $\beta$ -ME), and verified to be free of mycoplasma contamination. To induce pyroptosis, cells were stimulated with 10 ng/ml LPS plus 250 nM 5z7, 50 ng/ml TNF- $\alpha$  plus 250 nM 5z7, 1  $\mu$ g/ml LPS plus 20  $\mu$ M nigericin, or 2  $\mu$ g/ml PA plus 1  $\mu$ g/ml LFn-Fla. For noncanonical inflammasome activation, 2 million iBMDMs were mixed with 2  $\mu$ g of ultrapure LPS in 10  $\mu$ l of buffer R and electroporated using the Neon Transfection System (ThermoFisher Scientific) with parameters (1400 V, 10 ms, and 3 pulses). To induce apoptosis, iBMDMs were treated with 50  $\mu$ M etoposide. Transient transfection of HEK293T cells was performed with Lipofectamine 3000 (Invitrogen) according to the manufacturer's instructions. For stable transfection, lentiCas9-Blast, pHAGE-BSD-Flag, or pHAGE-Ble containing the gene of interest, together with packaging plasmids psPAX2 and pMD2.G in a ratio of 5:3:2, were transiently transfected into HEK293T cells. At 72 hours after transfection, the cell culture supernatant containing lentivirus was collected and filtered through a 0.45- $\mu$ m membrane (Millipore, #SLHV033RB) to remove cell debris. iBMDMs were then infected with the lentivirus for 3 days before adding 10  $\mu$ g/ml blasticidin or 400  $\mu$ g/ml zeocin for stable transfection selection.

#### Genome-wide CRISPR-Cas9 screen

The mouse CRISPR-knockout pooled library for genome-wide CRISPR/Cas9 screen was obtained from Addgene (#1000000053) and amplified according to the protocol provided by the manufacturer. For lentivirus production, mouse GeCKO A and B library plasmids were mixed equally and transfected into HEK293T cells together with the packaging plasmids psPAX2 and pMD2.G. Seventy-two hours later, lentivirus was collected and the viral titer was measured with the QuickTiter Lentivirus Titer kit (Cell Biolabs, #VPK-107). For the genome-wide screen, Cas9 stably expressing iBMDMs were seeded in 10-cm dishes

(2  $\times$  10<sup>6</sup> cells/dish), and 7  $\times$  10<sup>7</sup> cells were infected with the lentivirus-containing sgRNA library at a multiplicity of infection (MOI) of 0.3. Sixty hours later, cells were treated with puromycin to remove uninfected cells. Six days after that, the transduced cells were seeded in 40  $\times$  10 cm dishes (8  $\times$  10<sup>6</sup> cells/dish) and treated with 10 ng/ml LPS plus 125 nM 5z7 for 6 hours. Three days later, the surviving cells were reseeded and treated with 10 ng/ml LPS plus 250 nM 5z7 overnight. Two days later, surviving cells were again treated with 20 ng/ml LPS plus 250 nM 5z7 overnight before surviving cells were harvested. For the noncanonical inflammasome screen, 3  $\times$  10<sup>8</sup> transduced cells were electroporated with ultra LPS for three rounds. Surviving cells and untreated transduced cells (as the control sample) were harvested and lysed in the SNET buffer [20 mM Tris-HCl pH 8.0, 5 mM EDTA, 400 mM NaCl, 1% SDS and 400  $\mu$ g/ml Proteinase K (NEB, P8107S)]. Genomic DNAs were prepared by using phenol-chloroform extraction and isopropanol precipitation and amplified by two-step PCR using the 2 $\times$  HiEff Canace Gold PCR Master Mix (Yeasen, #10149ES01). The samples were quantified and sequenced on a HiSeq 2500 (Illumina) by GENEWIZ. Sequencing data were further processed and analyzed using the MAGeCK algorithm (37). MAGeCK built a linear model to estimate the variance of guide RNA (gRNA) read counts, evaluated the gRNA abundance changes between control and treatment conditions, and assigned *P* values for positive and negative selection.

#### Generation of knockout iBMDMs by CRISPR-Cas9

HEK293T cells were transfected with sgRNA-expressing lentiCRISPR v2 together with psPAX2 and pMD2.G at a ratio of 5:3:2. Then, 72 hours later, the supernatant containing lentivirus was collected and filtered through a 0.45- $\mu$ m membrane (Millipore) for subsequent iBMDM infection. Three days after infection, cells were treated with 5  $\mu$ g/ml puromycin before diluting to single clones cultured in 96-well plates. The candidate knockout clones were verified by sequencing of genomic DNA and immunoblot. sgRNA sequences for targeting the genes of interest were as follows: *Lamtor1* (5'-TGG ACC GGG CAA GGC AGT AC-3'/5'-GCT CTT CTT TCG CAT CCA CG-3'), *Lamtor4* (5'-AGC CAG TGC CAT CTC GGA GT-3'/5'-TAG ACT TCC GCA CTG ACC CA-3'), *Rragc* (5'-TTT CTG TAC CAC CTT ACT GA-3'/5'-TCA TAA GAC TGC ATA TCC AC-3'), *Flcn* (5'-GGC TGC CAG TCA CTT GCC GT-3'/5'-GCC TGC TAC CGC ATG CCT TC-3'), *Fnip2* (5'-ACC GTA TGT AGT GTA TCT TC-3'/5'-ACT TTA CTA ATC ATC AGT TG-3'), *Gsdmd* (5'-AGC ATC CTG GCA TTC CGA G-3'), *Nlrp3* (5'-GAA GAT TAC CCG CCC GAG AA-3'), and *Nlr4* (5'-TGT TTC GAA TAG TCC CCC CC-3').

#### Recombinant protein purification

PA and LFn-flagellin recombinant proteins were purified from Sf9 cells. Seventy-two hours after P3 baculovirus infection, cells were resuspended in lysis buffer (50 mM Tris-HCl, pH 8.0, 300 mM NaCl, 10 mM  $\beta$ -ME, 5 mM imidazole, and 1% Triton X-100) and then clarified by centrifugation at 42,000 rpm for 2 hours at 4°C. Proteins were purified using Ni-NTA agarose (QIAGEN), eluted with elution buffer (50 mM Tris-HCl pH 8.0, 300 mM NaCl, 10 mM  $\beta$ -ME, 500 mM imidazole), and further purified by Superdex 200 (10/300) gel-filtration chromatography and mono-Q ion exchange.

#### Bacterial strains and culture conditions

The *Y. pseudotuberculosis* YPIII strain, a gift from Dr. Shiyun Chen (Wuhan Institute of Virology, Chinese Academy of Sciences), was grown overnight in 2 $\times$  YT broth at 26°C. On the day of infection, bacteria were diluted 1:50 into 2 $\times$  YT plus 20 mM MgCl<sub>2</sub> and 20 mM sodium oxalate and grown for 2 hours at 26°C, followed by a shift to 37°C for 2 hours. Bacteria were then washed in phosphate-buffered saline (PBS; Invitrogen) and added to cells at a MOI of 40. Next, 100  $\mu$ g/ml gentamicin was added to the cultures 2 hours after infection. To quantify the number of bacteria that had been taken up by cells, iBMDMs were infected with the *Y. pseudotuberculosis* YPIII strain at the MOI indicated in the corresponding figures. Thirty minutes later, cells were washed with PBS three times and gentamicin was added to kill extracellular bacteria. Then, intracellular bacteria were released by treating cells with 0.05% Triton X-100 before lysates were serially diluted and plated on 2 $\times$  YT agar. Bacterial colonies were counted after 1 day of culture at 37°C. For the *Salmonella typhimurium* infection assay, bacteria were grown overnight in Luria-Bertani (LB) broth at 37°C. On the day of infection, bacteria were diluted 1:50 into LB broth and grown for 4 hours at 37°C. Bacteria were then washed with PBS and added to cells at a MOI of 20. Next, 100  $\mu$ g/ml gentamicin was added to the cultures 0.5 hours after infection to kill extracellular bacteria.

#### Cell death assays

Cell death and viability of stimulated macrophages were determined by measuring LDH release using the CytoTox 96 assay kit (Promega, #G1780) and ATP level using the CellTiter-Glo Luminescent Cell Viability Assay (Promega, #G7570), respectively. Luminescence and absorbance were measured on a BioTek Synergy H1 plate reader. For kinetic cytotoxicity assay by monitoring cell permeability, the cell culture medium was changed into buffer B [25 mM HEPES, pH 7.4, 120 mM NaCl, 4 mM KCl, 1.5 mM CaCl<sub>2</sub>, 1 mM MgCl<sub>2</sub>, 5mM glucose, 0.1% bovine serum albumin (BSA)] containing 2  $\mu$ g/ml PI (Invitrogen, #P3566), and the

fluorescence (excitation: 535 nm, emission: 617 nm) was continuously recorded after treatment for 5 hours at 30-min intervals using a BioTek Synergy plate reader.

### Immunoprecipitation and immunoblotting

For the immunoprecipitation assay, cells were harvested and resuspended in lysis buffer (50 mM Tris-HCl, pH 7.4, 150 mM NaCl, 1% Triton X-100) supplemented with a complete protease inhibitor cocktail (Sigma-Aldrich). Cell extracts were then incubated with the indicated antibodies for 4 hours at 4°C before adding protein A-G agarose beads for 2 hours. The beads were extensively washed at least three times with wash buffer (50 mM Tris-HCl, pH 7.4, 300 mM NaCl, 0.5% Triton X-100) and bound proteins were eluted by boiling with SDS-loading buffer. For immunoblot analysis, immunoprecipitation samples or whole-cell lysate samples were subjected to electrophoresis through SDS-polyacrylamide gel electrophoresis gels. The separated proteins were then transferred to a polyvinylidene fluoride membrane (Millipore). Immunoblot was probed with the indicated antibodies. The protein bands were visualized using a SuperSignal West Pico chemiluminescence ECL kit (Pierce).

### Immunostaining and confocal microscopy

iBMDMs grown on coverslips were stimulated with 10 ng/ml LPS plus 250 nM 5z7. Cells were fixed 100 min later with 4% paraformaldehyde for 20 min before permeabilization using 0.1% Triton X-100 (10 min) and blocking with 5% BSA (1 hour). Then, cells were immunostained with the indicated primary antibodies, followed by incubation with the corresponding fluorescent-conjugated secondary antibodies (Jackson ImmunoResearch). Nuclei were counterstained with 4,6-diamidino-2-phenylindole (DAPI; Cell Signaling Technology). Slides were mounted using Aqua-Poly/Mount (Dako). Images were captured using a Zeiss 880 laser scanning confocal microscope at 63× magnification and analyzed using Zeiss Zen software. Manders' overlap coefficient was calculated using ImageJ (where each point represents a single cell, with 100 cells per sample). All images are representative of at least three independent experiments.

### Statistics

Student's *t* test (two-tailed) was used for the statistical analysis of all experiments. *P* < 0.05 was considered significant.

### REFERENCES AND NOTES

1. P. Broz, V. M. Dixit, Inflammasomes: Mechanism of assembly, regulation and signalling. *Nat. Rev. Immunol.* **16**, 407–420 (2016). doi: [10.1038/nri.2016.58](https://doi.org/10.1038/nri.2016.58); pmid: [27291964](https://pubmed.ncbi.nlm.nih.gov/27291964/)
2. N. M. de Vasconcelos, M. Lamkanfi, Recent insights on inflammasomes, gasdermin pores, and pyroptosis. *Cold Spring Harb. Perspect. Biol.* **12**, a036392 (2020). doi: [10.1101/cshperspect.a036392](https://doi.org/10.1101/cshperspect.a036392); pmid: [31570336](https://pubmed.ncbi.nlm.nih.gov/31570336/)
3. D. R. Green, The coming decade of cell death research: Five riddles. *Cell* **177**, 1094–1107 (2019). doi: [10.1016/j.cell.2019.04.024](https://doi.org/10.1016/j.cell.2019.04.024); pmid: [31100266](https://pubmed.ncbi.nlm.nih.gov/31100266/)
4. N. Kayagaki et al., Caspase-11 cleaves gasdermin D for non-canonical inflammasome signalling. *Nature* **526**, 666–671 (2015). doi: [10.1038/nature15541](https://doi.org/10.1038/nature15541); pmid: [26375259](https://pubmed.ncbi.nlm.nih.gov/26375259/)
5. J. Shi et al., Cleavage of GSDMD by inflammatory caspases determines pyroptotic cell death. *Nature* **526**, 660–665 (2015). doi: [10.1038/nature15514](https://doi.org/10.1038/nature15514); pmid: [26375003](https://pubmed.ncbi.nlm.nih.gov/26375003/)
6. J. Ding et al., Pore-forming activity and structural autoinhibition of the gasdermin family. *Nature* **535**, 111–116 (2016). doi: [10.1038/nature18590](https://doi.org/10.1038/nature18590); pmid: [27281216](https://pubmed.ncbi.nlm.nih.gov/27281216/)
7. X. Liu et al., Inflammasome-activated gasdermin D causes pyroptosis by forming membrane pores. *Nature* **535**, 153–158 (2016). doi: [10.1038/nature18629](https://doi.org/10.1038/nature18629); pmid: [27383986](https://pubmed.ncbi.nlm.nih.gov/27383986/)
8. L. Sborgi et al., GSDMD membrane pore formation constitutes the mechanism of pyroptotic cell death. *EMBO J.* **35**, 1766–1778 (2016). doi: [10.15252/emj.201694696](https://doi.org/10.15252/emj.201694696); pmid: [27418190](https://pubmed.ncbi.nlm.nih.gov/27418190/)
9. R. A. Aglietti et al., GsdmD p30 elicited by caspase-11 during pyroptosis forms pores in membranes. *Proc. Natl. Acad. Sci. U.S.A.* **113**, 7858–7863 (2016). doi: [10.1073/pnas.1607769113](https://doi.org/10.1073/pnas.1607769113); pmid: [27339137](https://pubmed.ncbi.nlm.nih.gov/27339137/)
10. R. Heilig et al., The Gasdermin-D pore acts as a conduit for IL-1 $\beta$  secretion in mice. *Eur. J. Immunol.* **48**, 584–592 (2018). doi: [10.1002/eji.201747404](https://doi.org/10.1002/eji.201747404); pmid: [29274245](https://pubmed.ncbi.nlm.nih.gov/29274245/)
11. C. L. Evavold et al., The pore-forming protein Gasdermin D regulates interleukin-1 secretion from living macrophages. *Immunity* **48**, 35–44.e6 (2018). doi: [10.1016/j.immuni.2017.11.013](https://doi.org/10.1016/j.immuni.2017.11.013); pmid: [29195811](https://pubmed.ncbi.nlm.nih.gov/29195811/)
12. P. Orning et al., Pathogen blockade of TAK1 triggers caspase-8-dependent cleavage of gasdermin D and cell death. *Science* **362**, 1064–1069 (2018). doi: [10.1126/science.aau2818](https://doi.org/10.1126/science.aau2818); pmid: [30361383](https://pubmed.ncbi.nlm.nih.gov/30361383/)
13. J. Sarhan et al., Caspase-8 induces cleavage of gasdermin D to elicit pyroptosis during *Yersinia* infection. *Proc. Natl. Acad. Sci. U.S.A.* **115**, E10888–E10897 (2018). doi: [10.1073/pnas.1809548115](https://doi.org/10.1073/pnas.1809548115); pmid: [30381458](https://pubmed.ncbi.nlm.nih.gov/30381458/)
14. N. Kayagaki et al., IRF2 transcriptionally induces GSDMD expression for pyroptosis. *Sci. Signal.* **12**, eaax4917 (2019). doi: [10.1126/scisignal.aax4917](https://doi.org/10.1126/scisignal.aax4917); pmid: [31113851](https://pubmed.ncbi.nlm.nih.gov/31113851/)
15. L. Bar-Peled, D. M. Sabatini, Regulation of mTORC1 by amino acids. *Trends Cell Biol.* **24**, 400–406 (2014). doi: [10.1016/j.tcb.2014.03.003](https://doi.org/10.1016/j.tcb.2014.03.003); pmid: [24698685](https://pubmed.ncbi.nlm.nih.gov/24698685/)
16. J. Hirst, Mitochondrial complex I. *Annu. Rev. Biochem.* **82**, 551–575 (2013). doi: [10.1146/annurev-biochem-070511-103700](https://doi.org/10.1146/annurev-biochem-070511-103700); pmid: [23527692](https://pubmed.ncbi.nlm.nih.gov/23527692/)
17. C. Rogers et al., Gasdermin pores permeabilize mitochondria to augment caspase-3 activation during apoptosis and inflammasome activation. *Nat. Commun.* **10**, 1689 (2019). doi: [10.1038/s41467-019-09397-2](https://doi.org/10.1038/s41467-019-09397-2); pmid: [30976076](https://pubmed.ncbi.nlm.nih.gov/30976076/)
18. W. J. Kaiser et al., RIP3 mediates the embryonic lethality of caspase-8-deficient mice. *Nature* **471**, 368–372 (2011). doi: [10.1038/nature09857](https://doi.org/10.1038/nature09857); pmid: [21368762](https://pubmed.ncbi.nlm.nih.gov/21368762/)
19. A. Oberst et al., Catalytic activity of the caspase-8-FLIP(L) complex inhibits RIPK3-dependent necrosis. *Nature* **471**, 363–367 (2011). doi: [10.1038/nature09852](https://doi.org/10.1038/nature09852); pmid: [21368763](https://pubmed.ncbi.nlm.nih.gov/21368763/)
20. D. Vercammen et al., Inhibition of caspases increases the sensitivity of L929 cells to necrosis mediated by tumor necrosis factor. *J. Exp. Med.* **187**, 1477–1485 (1998). doi: [10.1084/jem.187.9.1477](https://doi.org/10.1084/jem.187.9.1477); pmid: [9565639](https://pubmed.ncbi.nlm.nih.gov/9565639/)
21. S. Nada et al., The novel lipid raft adaptor p18 controls endosome dynamics by anchoring the MEK-ERK pathway to late endosomes. *EMBO J.* **28**, 477–489 (2009). doi: [10.1038/emboj.2008.308](https://doi.org/10.1038/emboj.2008.308); pmid: [19177150](https://pubmed.ncbi.nlm.nih.gov/19177150/)
22. Y. Sancak et al., Regulator-Rag complex targets mTORC1 to the lysosomal surface and is necessary for its activation by amino acids. *Cell* **141**, 290–303 (2010). doi: [10.1016/j.cell.2010.02.024](https://doi.org/10.1016/j.cell.2010.02.024); pmid: [20381137](https://pubmed.ncbi.nlm.nih.gov/20381137/)
23. H. I. Muendlein et al., ZBP1 promotes LPS-induced cell death and IL-1 $\beta$  release via RHIM-mediated interactions with RIPK1. *Nat. Commun.* **12**, 86 (2021). doi: [10.1038/s41467-020-20357-z](https://doi.org/10.1038/s41467-020-20357-z); pmid: [33397971](https://pubmed.ncbi.nlm.nih.gov/33397971/)
24. H. I. Muendlein et al., cFLIP<sub>L</sub> protects macrophages from LPS-induced pyroptosis via inhibition of complex II formation. *Science* **367**, 1379–1384 (2020). doi: [10.1126/science.aay3878](https://doi.org/10.1126/science.aay3878); pmid: [32193329](https://pubmed.ncbi.nlm.nih.gov/32193329/)
25. I. Matsuda et al., The C-terminal domain of the long form of cellular FLICE-inhibitory protein (c-FLIP<sub>L</sub>) inhibits the interaction of the caspase 8 prodomain with the receptor-interacting protein 1 (RIP1) death domain and regulates caspase 8-dependent nuclear factor  $\kappa$ B (NF- $\kappa$ B) activation. *J. Biol. Chem.* **289**, 3876–3887 (2014). doi: [10.1074/jbc.M113.506485](https://doi.org/10.1074/jbc.M113.506485); pmid: [24398693](https://pubmed.ncbi.nlm.nih.gov/24398693/)
26. Y. H. Park, M. S. Jeong, H. H. Park, S. B. Jang, Formation of the death domain complex between FADD and RIP1 proteins in vitro. *Biochim. Biophys. Acta* **1834**, 292–300 (2013). doi: [10.1016/j.bbapap.2012.08.013](https://doi.org/10.1016/j.bbapap.2012.08.013); pmid: [22922561](https://pubmed.ncbi.nlm.nih.gov/22922561/)
27. H. Anderton et al., RIPK1 prevents TRADD-driven, but TNFR1 independent, apoptosis during development. *Cell Death Differ.* **26**, 877–889 (2019). doi: [10.1038/s41418-018-0166-8](https://doi.org/10.1038/s41418-018-0166-8); pmid: [30185824](https://pubmed.ncbi.nlm.nih.gov/30185824/)
28. M. Muzio et al., FLICE, a novel FADD-homologous ICE/CED-3-like protease, is recruited to the CD95 (Fas/APO-1) death-inducing signaling complex. *Cell* **85**, 817–827 (1996). doi: [10.1016/S0092-8674\(00\)81266-0](https://doi.org/10.1016/S0092-8674(00)81266-0); pmid: [8681377](https://pubmed.ncbi.nlm.nih.gov/8681377/)
29. T. M. Fu et al., Cryo-EM structure of caspase-8 tandem DED filament reveals assembly and regulation mechanisms of the death-inducing signaling complex. *Mol. Cell* **64**, 236–250 (2016). doi: [10.1016/j.molcel.2016.09.009](https://doi.org/10.1016/j.molcel.2016.09.009); pmid: [27746017](https://pubmed.ncbi.nlm.nih.gov/27746017/)
30. K. Shen et al., Cryo-EM structure of the human FLCN-FNIP2-Rag-Regulator complex. *Cell* **179**, 1319–1329.e8 (2019). doi: [10.1016/j.cell.2019.10.036](https://doi.org/10.1016/j.cell.2019.10.036); pmid: [31704029](https://pubmed.ncbi.nlm.nih.gov/31704029/)
31. C. C. Thoren et al., An ATP-competitive mammalian target of rapamycin inhibitor reveals rapamycin-resistant functions of mTORC1. *J. Biol. Chem.* **284**, 8023–8032 (2009). doi: [10.1074/jbc.M900301200](https://doi.org/10.1074/jbc.M900301200); pmid: [19150980](https://pubmed.ncbi.nlm.nih.gov/19150980/)
32. R. E. Lawrence et al., Structural mechanism of a Rag GTPase activation checkpoint by the lysosomal folliculin complex. *Science* **366**, 971–977 (2019). doi: [10.1126/science.aax0364](https://doi.org/10.1126/science.aax0364); pmid: [31672913](https://pubmed.ncbi.nlm.nih.gov/31672913/)
33. G. Napolitano et al., A substrate-specific mTORC1 pathway underlies Birt-Hogg-Dubé syndrome. *Nature* **585**, 597–602 (2020). doi: [10.1038/s41586-020-2444-0](https://doi.org/10.1038/s41586-020-2444-0); pmid: [32612235](https://pubmed.ncbi.nlm.nih.gov/32612235/)
34. L. Bar-Peled, L. D. Schweitzer, R. Zoncu, D. M. Sabatini, Regulator is a GEF for the rag GTPases that signal amino acid levels to mTORC1. *Cell* **150**, 1196–1208 (2012). doi: [10.1016/j.cell.2012.07.032](https://doi.org/10.1016/j.cell.2012.07.032); pmid: [22980980](https://pubmed.ncbi.nlm.nih.gov/22980980/)
35. Z. Y. Tsun et al., The folliculin tumor suppressor is a GAP for the RagC/D GTPases that signal amino acid levels to mTORC1. *Mol. Cell* **52**, 495–505 (2013). doi: [10.1016/j.molcel.2013.09.016](https://doi.org/10.1016/j.molcel.2013.09.016); pmid: [24095279](https://pubmed.ncbi.nlm.nih.gov/24095279/)
36. N. M. de Vasconcelos, N. Van Opendenbosch, H. Van Gorp, E. Parthoens, M. Lamkanfi, Single-cell analysis of pyroptosis dynamics reveals conserved GSDMD-mediated subcellular events that precede plasma membrane rupture. *Cell Death Differ.* **26**, 146–161 (2019). doi: [10.1038/s41418-018-0106-7](https://doi.org/10.1038/s41418-018-0106-7); pmid: [29666477](https://pubmed.ncbi.nlm.nih.gov/29666477/)
37. W. Li et al., Quality control, modeling, and visualization of CRISPR screens with MAGeCK-VISPR. *Genome Biol.* **16**, 281 (2015). doi: [10.1186/s13059-015-0843-6](https://doi.org/10.1186/s13059-015-0843-6); pmid: [26673418](https://pubmed.ncbi.nlm.nih.gov/26673418/)

### ACKNOWLEDGMENTS

We thank S. Chen (Wuhan Institute of Virology, Chinese Academy of Sciences, China) for providing the *Y. pseudotuberculosis* YPIII strain and Z. Du (Beijing Institute of Microbiology and Epidemiology, China) for sharing anti-YopJ antibody. **Funding:** This work was supported by National Key R&D Program of China (2020YFA0509600), Key Research Program of the Chinese Academy of Sciences (ZDBS-LY-SM008), National Natural Science Foundation of China (31972897), Strategic Priority Research Program of Chinese Academy of Sciences (XDB29030300), Shanghai Municipal Science and Technology Major Project (2019SHZDZX02) to X.L., National Natural Science Foundation of China for the Youth (31900456) to Ze.Z., and NIH R01 CA240955 to J.L. **Author contributions:** Ze.Z., W.D., Y.B., R.Mia., J.L. and X.L. conceived the study. Ze.Z., W.D., Y.B., and R.Mia. designed and performed most experiments with assistance from R.Min, F.D., Z.W., W.L., and P.C.; Ze.Z. and S.M. performed the CRISPR screen and sequencing data analysis, respectively. Zh.Z., Y.P., Y.W., T.M., and X.W.L. provided technical support. Ze.Z., W.D., Y.B., R.Mia., J.L., and X.L. analyzed the data and wrote the manuscript. X.L. supervised the study. **Competing interests:** The authors declare no competing interests. **Data and materials availability:** All data are available in the main text or the supplementary materials.

### SUPPLEMENTARY MATERIALS

[science.sciencemag.org/content/372/6549/eabg0269/suppl/DC1](https://science.sciencemag.org/content/372/6549/eabg0269/suppl/DC1)  
Figs. S1 to S12  
MDAR Reproducibility Checklist

[View/request a protocol for this paper from Bio-protocol.](https://www.biorxiv.org/request-a-protocol)

14 December 2020; resubmitted 4 April 2021  
Accepted 18 May 2021  
[10.1126/science.abg0269](https://doi.org/10.1126/science.abg0269)

## The lysosomal Rag-Ragulator complex licenses RIPK1– and caspase-8–mediated pyroptosis by *Yersinia*

Zengzhang ZhengWanyan DengYang BaiRui MiaoShenglin MeiZhibin ZhangYoudong PanYi WangRui MinFan DengZeyu WuWu LiPengcheng ChenTianchi MaXiwen LouJudy LiebermanXing Liu

*Science*, 372 (6549), eabg0269. • DOI: 10.1126/science.abg0269

### Cell death limits pathogens

During infection, *Yersinia* inhibition of the protein kinase TAK1 triggers cleavage of the pore-forming protein gasdermin D (GSDMD), which leads to a kind of inflammatory cell death called pyroptosis. In a genome-wide screen, Zheng *et al.* identified a lysosome-tethered regulatory supercomplex as being a critical driver of *Yersinia*-induced pyroptosis. The activity of the GTPase Rag and lysosomal tethering of Rag-Ragulator were required to recruit and activate the kinase RIPK1 and protease caspase-8 to cleave GSDMD, which causes cell death and limits infection. By contrast, Rag-Ragulator was not required for inflammasome-mediated pyroptosis. Thus, metabolic signaling on lysosomes can regulate cell death during pathogenic bacterial infection.

*Science*, abg0269, this issue p. eabg0269

### View the article online

<https://www.science.org/doi/10.1126/science.abg0269>

### Permissions

<https://www.science.org/help/reprints-and-permissions>

Use of this article is subject to the [Terms of service](#)

*Science* (ISSN 1095-9203) is published by the American Association for the Advancement of Science. 1200 New York Avenue NW, Washington, DC 20005. The title *Science* is a registered trademark of AAAS.

Copyright © 2021 The Authors, some rights reserved; exclusive licensee American Association for the Advancement of Science. No claim to original U.S. Government Works